Istraživanja i projektovanja za privredu
ISSN 1451-4117
DOI:10.5937/jaes0-43777
www.engineeringscience.rs

iipp publishing

Journal of Applied Engineering Science
Vol. 21, No. 3, 2023
Original Scientific Paper
Paper number: 21(2023)3, 1130, 884-895

BEHAVIOR OF GEOPOLYMER CONCRETE WALL PANELS WITH SQUARE OPENING VARIATIONS SUBJECTED TO CYCLIC LOADS

Saloma[1], Siti Aisyah Nurjannah[1]*, Hanafiah[1], Arie Putra Usman[1], Steven Hu[1], Fathoni Usman[2]

[1] Department of Civil Engineering, Universitas Sriwijaya, Palembang, Indralaya, Indonesia
[2] Department of Institute of Energy Infrastructure, Universiti Tenaga Nasional, 43000 Kajang, Selangor, Malaysia
** sitiaisyahn@ft.unsri.ac.id*

Masonry walls are non-structural elements that can increase the stiffness and strength of building structures subjected to lateral loads. Reinforced concrete (RC) wall systems are structural elements that have been developed to improve structural performance. Because the use of large amounts of cement in RC is not environmentally friendly, cement-free concrete called geopolymer concrete (GC) has been developed. Research on GC structural beam-column joints and slab joints has proven that GC fulfils the strength requirements for structural elements. However, previous studies have not addressed the performance of reinforced GC wall panels (WPs) under cyclic loads. Therefore, this study filled the gap with the novelty of investigating the performance of reinforced GC structural WPs subjected to cyclic lateral loads. Numerical analysis was used to determine the performance of GC-WPs in resisting cyclic lateral loads, and an aerated concrete wall panel (AC-WP) model was used for verification. The study investigated GC-WPs that were 1500 mm wide and 200 mm thick, varying in solidity such that one was entirely solid (GC-WP1) and two had square openings in horizontal and vertical configurations (GC-WP2 and GC-WP3, respectively). The cyclic loading history referenced FEMA 461. The analysis resulted in hysteretic curves, ductility ratios, and stress contours. GC-WP1 achieved the highest maximum lateral loads (73,994 kN and -67,225 kN) compared to the other GC-WP models, with a high ductility ratio of 14,681. Results show that GC has the potential for use in WPs to improve their resistance to lateral cyclic loads.

Keywords: cyclic lateral loads, finite element method, geopolymer concrete, wall panel

1 INTRODUCTION

Structural elements of buildings serve as load supports, while non-structural elements are designed to provide additional strength to structural components. Masonry walls are examples of a non-structural element often found in buildings as a partition between rooms. Although they are non-structural elements, these walls provide additional rigidity to open frames and reduce displacement of the columns and beams when the structure is required to resist lateral cyclic loads caused by earthquakes. Various wall panel (WP) systems have been developed to increase buildings' structural performance in reducing lateral displacement. WP walls are one such technological development in the construction sector. They are projected to replace conventional masonry walls owing to the advantages they provide, such as reduced weight (due to being thinner than conventional masonry walls) and shortened installation-time.

The widespread use of cement in the construction sector results in the emission of CO_2 which causes environmental damage. Research on environmentally-friendly concrete has been carried out to address this problem. One environmentally-sustainable concrete type is geopolymer concrete (GC), which studies have shown can substitute fly ash for cement [1,2]. Moreover, as the fly and bottom ash that GC incorporates are both residual wastes from coal combustion, repurposing these as a component of GC reduces overall industrial waste. Fly ash has a finer grain size than bottom ash, with a resultant lighter density. It contains silica, aluminum, iron, calcium, and other oxides at lesser levels, making it similar to cement. As such, fly ash forms a viable cement substitute. Concrete contains cement, fine aggregate, coarse aggregate, and additive materials. Its strength is supported by the coarse aggregate. The spaces between the coarse aggregate elements are filled by fine aggregate. Cement is usually used as a binder to bond the two fillers. GC binds material (although not completely) using Portland cement. It uses a polymerization reaction in which aluminum and silica compounds mixed with an alkaline solution produce a long series of AlO_4 and SiO_4 [3].

Research indicates that a high-density geopolymer nanocomposite that incorporates basalt fiber, coal ash, and nano sodium oxide achieves the best interfacial zone and polymer-reaction performance owing to the possession of nanocomposites containing 3% nano sodium oxide [4]. Micro-carbon fly-ash-based geopolymer pastes have been developed using nano titanium dioxide at concentrations of 2% to improve flexural strength and fracture toughness, and 3% to enhance compactness and compressive strength [5].

Previous studies discussed the potential of GC for use in structural elements and geopolymer mortar as a retrofitting material. Two GC interior beam-column and six GC exterior beam-column joint specimens were tested against cyclic lateral loads. The GC materials used slag as a binder and fly ash to increase stability and microstructure. Under ultimate (final) conditions, bar bonds in specimens with a ratio of column cross-sectional height (h_c) to beam cross-sectional height (d_b) of 25 or more showed better performance than specimens with an h_c/d_b ratio of less than 25. All specimens experienced a pinching effect due to connection types at the beam-column joints comprising straight bars, hooked bars, and headed bars [6].

Nine beams and seven columns of reinforced concrete and geopolymer sea-sand concrete were tested for bending and axial compression. In this study, the GC material incorporated M_gO from sea sand and was used to prevent shrinkage. Results showed that using a combination of GC materials and basalt-fiber-reinforced polymer for beams and columns resulted in a higher capacity to withstand loads than other GC steel-bar-reinforced specimens with the same reinforcement ratio. The strength of beams and columns was shown to increase concomitantly with the reinforcement ratio [7].

Geopolymer and steel-fiber geopolymer mortars were applied as retrofit materials to beam-column joint specimens damaged due to cyclic loads. After the damaged parts were removed and replaced with both types of mortar, a cyclic load was applied to the beam-column joint specimens. Analysis of the test results indicated that all retrofitted specimens achieved the same performance as the control specimens in strength, ductility, energy dissipation, and stiffness [8].

Twelve one-way slabs, consisting of six specimens made of GC and six of Ordinary Portland Cement-based (OPC-based) concrete, were tested against bending loads. The GC material contained slag and fly ash and had been cured under ambient conditions. The load-induced crack width and spacing were smaller in all the GC slab specimens due to the high bond strength between the rebar and the GC. GC materials demonstrated lower crack load and initial stiffness than the OPC-based concrete specimens [9].

One-way concrete slabs strengthened by textile-reinforced geopolymer mortar were subjected to flexural testing. Results showed that the strengthening postponed the crack propagation and escalated the stiffness and flexural capacity. The increased number of strengthening layers accounted for the enhanced flexural capacity. All strengthened slabs performed better than the polymer-mortar-based slabs in terms of flexural capacity and crack width [10].

An investigation of geopolymer mortar materials as wall components subjected eighteen reinforced concrete infilled-frame specimens measuring 700 × 700 × 65 mm to diagonal compression loads. The results indicated that the performance of infilled frames using geopolymer-based mortar as a brick binder for retrofitting was better than that of frames using cement-based mortar. The specimens using geopolymer mortar material did not experience significant damage, whereas the cement-based mortar specimens experienced shear failure due to the main diagonal crack [11].

A geopolymer mortar reinforced with carbon, glass, and polypropylene fibers was applied to masonry wall specimens. Sodium silicate and sodium hydroxide were used as alkali activators to manufacture the geopolymer mortar. Masonry-wall specimens with a 700 × 700 cm height and width were tested by the diagonal application of a compressive load to each. The specimens using fiber-geopolymer mortar achieved better shear strength in the uniaxial compression tests, as well as higher axial bearing capacity and ductility ratios in diagonal compression tests [12].

Openings in WPs have been shown to affect the load capacity they can resist and influence the crack patterns. In a previous study [13], a D2R01 WP specimen was displaced 95.3125 mm due to a push load of 87.3 kN and a drift ratio of 6.5%. The maximum pull load was 67 kN, with a displacement of 95.3125 mm and a drift ratio of 6.5%. In a study of sandwich wall panels (SWPs) using GC material [14], two variants of the SWPs (squat and slender) with were subjected to concentrically and eccentrically axial loads. The squat SWP dimensions were 2240 mm height, 400 mm width, and 11.2 slenderness ratio, while the slender SWP dimensions were 3440 mm height, 400 mm width, and 17.2 slenderness ratio. The test results revealed that the axial load capacity changed gradually. The raised ratio of load eccentricity to the cross-sectional thickness reduced the axial load capacity compared with the axial concentrically-loaded counterparts. GC crushing affected the final condition of both variants of SWPs. The slender SWPs were more stable than their squat counterparts when subjected to axial loads with large eccentricities. The opposite behavior was exhibited when the slender SWPs were subjected to axial loads with small eccentricities. In another study, four precast WPs were connected and subjected to cyclic loading to analyze seismic performance [15]. Variations in stirrup spacing, bolt diameter, steel plate thickness, and panel height-to-width ratios were included for testing. Results revealed a gradual performance increment for the bolt-connected WPs. WPs with closely-spaced stirrups required thicker connecting steel plates and more high-performance bolts.

1.1 Research significance

Although extensive investigation into the application of GC to WP structural elements is required for proper understanding of its performance, research on the topic has not been considered. This study attempts to address is by the conduction of a novel investigation into the behavior and performance of structural WPs using GC subjected to cyclic lateral loads. The WPs in the study were composed of GC containing fly ash as an environmentally-friendly substitute for cement. The purpose of the study was to determine the behavior of WPs made of GC with and without various square openings in horizontal and vertical configurations, subjected to lateral cyclic loads. The research was conducted using a numerical modeling approach that provides valuable information for both predicting a structural element's performance and understanding its behavior [16,17,18]. ANSYS v.19 was the software used to generate WP models and perform numerical analysis based on the finite element method. A structural case was categorized as nonlinear if the stiffness and load matrices' values depended on the displacement. Nonlinearity of two types was considered, specifically material nonlinearity and element geometry nonlinearity. The values produced depended on material data, such as plasticity in material nonlinearity and element configuration in element geometry nonlinearity. In some cases, a three-stage linear approach (divided into preprocessing, solution, and postprocessing) facilitated

problem-solving. The outputs of the numerical modeling were hysteretic curves, stress contours, and ductility values. The results of this study provide information about the performance of GC structural WPs, showing that applying GC materials in precast WPs can decrease the duration of construction work and achieve greater environmental friendliness by reducing CO_2 emissions.

2 MATERIALS AND METHOD

Two types of materials were used in the study, aerated concrete (AC) and geopolymer concrete (GC). Four models (AC-WP, GC-WP1, GC-WP2, and GC-WP3) were studied. The AC-WP model used AC for the WP, while the GC-WP1, GC-WP2, and GC-WP3 models used GC. The AC was strengthened by textile fibers and demonstrated a 17.5 MPa compressive strength and a 19662 MPa modulus of elasticity [13]. Previous research [19] supplied the GC properties: compressive strength, flexural strength, and an elastic modulus of 41.47 MPa, 9.21 MPa, and 30266 MPa, respectively. The GC incorporated fly ash as a precursor, a 0.5% fraction by volume of 30 mm pineapple fibers, fine aggregate with 5% $NaOH$ 16 M solutions, and 10% Na_2SiO_3 as alkali activators. All WP model dimensions were drawn from previous research [13]: a length of 1.5 meters, a thickness of 0.2 meters, and a width of 1.5 meters. The AC-WP and GC-WP1 models were solid, while the GC-WP2 and GC-WP3 models had two horizontal rectangular and two vertical rectangular openings, respectively, based on previous research [20]. The dimensions of the WPs and the openings are detailed in Figs. 1 to 3 with further details in Table 1.

The actual lateral-loading conditions used in the study are depicted in Fig. 4. The supports and load locations were set in accordance with those of [13]. Each WP numerical model was subjected to cyclic lateral loads based on the code [21] and applied to the top left side. This corresponds to the actuator and load cell positions, which were supported by the reaction wall in the experimental work. The WP specimens were modeled numerically to be of identical sizes, with fixed-end restraints as their bases. The displacement values usually detected in the laboratory using Linear Variable Displacement Transducers were used as input for the numerical modeling based on displacement controls.

Table 1. Wall panel dimension

Model	Material	Length	Width	Thickness	Opening	Opening position	Clear distance
AC-WP	AC	1500	1500	200	-	-	-
GC-WP1	GC	1500	1500	200	-	-	-
GC-WP2	GG	1500	1500	200	300 × 300	Horizontal	300
GC-WP3	GC	1500	1500	200	300 × 300	Vertical	300

Note: dimension in mm; AC: aerated concrete; GC: geopolymer concrete

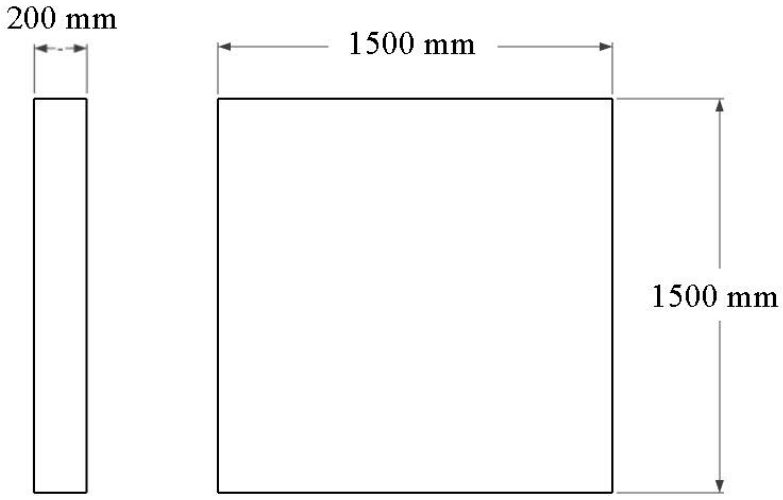

Fig. 1. Details of AC-WP and GC-WP1 models

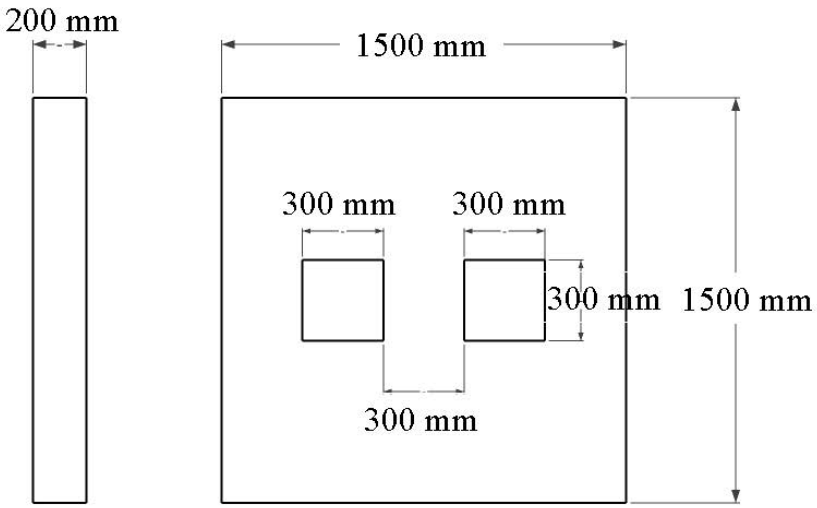

Fig. 2. Details of GC-WP2 model

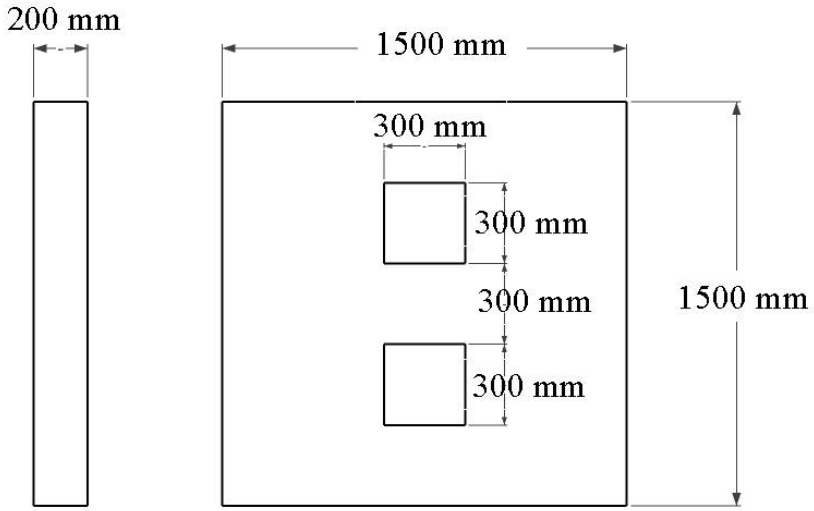

Fig. 3. Details of GC-WP3 model

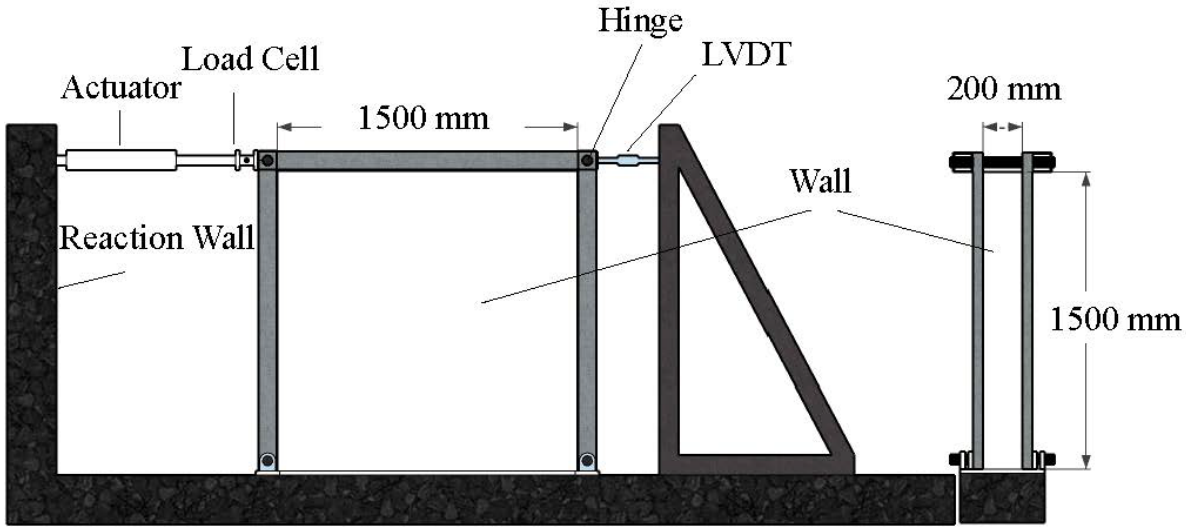

Fig. 4. Lateral loading setup

Several elements were used by the ANSYS software in the numerical modeling process. The element “Solid65” comprised eight nodes connected by edges to form a subdomain. It behaved similarly to concrete, displaying high compressive and low tensile strength. The element “Solid45” also comprised eight nodes, and represented steel elements with high ductility and high tensile strength. Finally, “Link180” elements consisted of only two nodes representing steel bars with high ductility [22]. The data input into the ANSYS software were the dimensions of the

WPs, the concrete properties (modulus elasticity, stress-strain, and tensile strength), steel-bar properties (diameter, modulus elasticity, and stress-strain), and steel-plate properties (modulus elasticity and stress-strain). The provision of cyclic loads is drawn from [21]. From [23,24], hysteretic curves' first, second, and third cycles performed relatively similarly. As such, the software only needed one load cycle to determine the hysteretic curves. The loading history used in this study is depicted in Fig. 5. The hysteretic curves provide some information, including ductility, that can be obtained using Equation (1) [25,26].

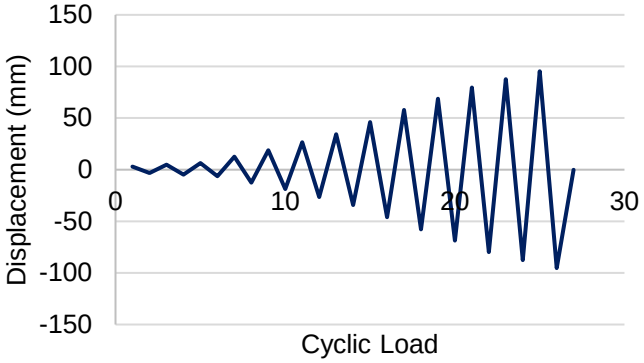

Fig. 5. Cyclic loading history

$$\mu_{\Delta} = \Delta_{ultimate}/\Delta_{yield} \quad (1)$$

where μ_{Δ}, $\Delta_{ultimate}$, and Δ_{yield} are ductility, ultimate, and yield displacements, respectively.

The flow chart of the work steps of this study is depicted in Fig. 6.

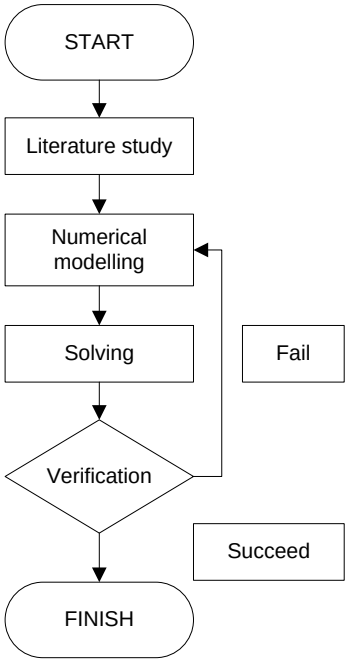

Fig. 6. Work steps

3 RESULTS AND DISCUSSSION

Verification aims to determine the difference between the experimental results and the numerical modeling results from the ANSYS simulation. The greatest lateral forces for push and pull loads on the AC-WP as determined from simulation and experiment were compared, demonstrating differences of less than 10% within range for the required accuracy [27], as presented in Table 2. The damage owing to push loads resulted in decreased stiffness and strength. Subsequently, when the specimen resisted the pull load, this resulted in a lower drift ratio under the maximum load. The difference in maximum loads in the experiment was owing to shear failure under maximum push load, indicated by a wide diagonal crack. Consequently, the shear capacity of the WP decreased significantly, resulting in a lower maximum pull load [13]. Table 3 lists the drift ratios at maximum loads. The unbalanced shear failure did not occur in the numerical simulation. All elements experienced damage distributed over push and pull loads and reached the same drift ratios at maximum loads. Table 4 gives the ultimate drift ratios at the end of the loading process. The AC-WP model and specimen achieved the same ultimate drift ratio of 6.48%.

Table 2. Percentage of maximum lateral force difference between experiment and simulation for AC-WP

Load Direction	Maximum load (kN)		Difference (%)
	Simulation	Experiment	
Push	81.40	87.30	6.758
Pull	-72.56	-66.04	9.871

Table 3. Drift ratios at maximum loads

Load Direction	Drift Ratio (%) at maximum loads	
	Simulation	Experiment
Push	1.771	2.133
Pull	1.771	1.733

Table 4. Ultimate drift ratios

Load Direction	Ultimate drift ratio (%)	
	Simulation	Experiment
Push	6.48	6.48
Pull	6.48	6.48

Figure 7 shows the hysteretic curve of the AC-WP model, which satisfies the accuracy criteria listed in Table 2. The GC-WP1, GC-WP2, and GC-WP3 models bore lateral loads based on the same loading history as the AC-WP specimen, as depicted in Fig. 5. Figures 8, 9, and 10 show the obtained hysteretic curves. The shapes of these curves indicate that all the WP models experienced a dominant shear mechanism. All GC-WP models achieved the same ultimate drift of 6.476% under push and pull loads, indicating the same high-ductility behavior. GC-WP1 (the solid WP) reached the highest maximum lateral loads, followed by GC-WP3 (two vertical openings) and GC-WP2 (two horizontal openings). The order of the highest maximum loads represented the stiffnesses of the WPs [28]. The two horizontal openings were shown to decrease stiffness significantly compared to the two vertical openings. GC-WP1 achieved the highest maximum lateral loads, due to its solidity providing the highest stiffness. The comparison of maximum lateral loads, drift ratios at maximum lateral loads, and ultimate drift ratios obtained from the experiment [13] and simulation are listed in Tables 5, 6, and 7.

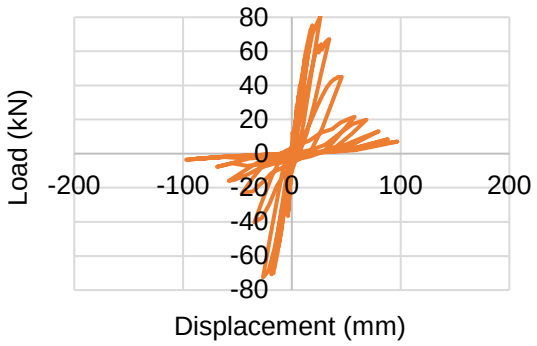

Fig. 7. Hysteretic curves of AC-WP model

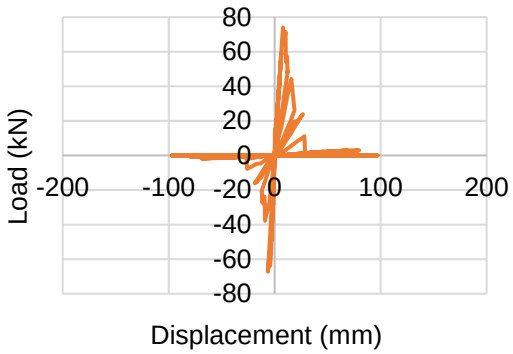

Fig. 8. Hysteretic curves of GC-WP1 model

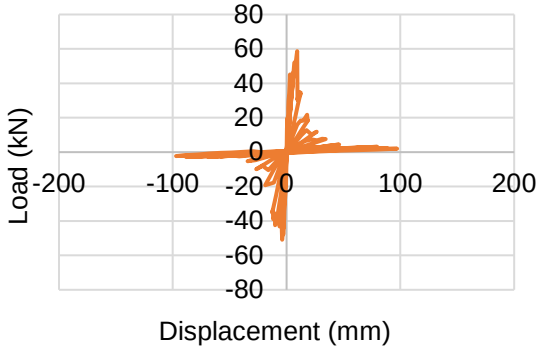

Fig. 9. Hysteretic curves of GC-WP2 model

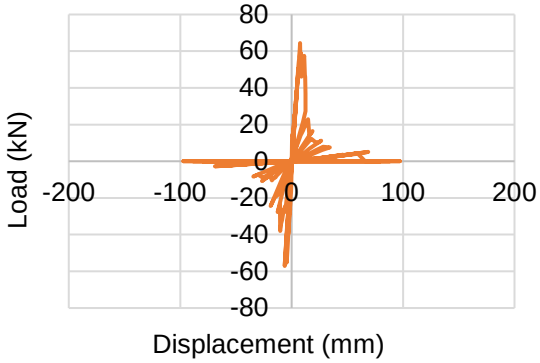

Fig. 10. Hysteretic curves of GC-WP3 model

Table 5. Maximum lateral loads

Load direction	Maximum lateral loads (kN)				
	Experiment	Simulation of models			
	AC-WP	AC-WP	GC-WP1	GC-WP2	GC-WP3
Push	90	81.401	73.994	58.686	64.418
Pull	-67	-72.559	-67.225	-50.904	-57.069

Table 6. Drift ratios at maximum lateral loads

Load direction	Drift ratio (%) at maximum lateral load				
	Experiment	Simulation of models			
	AC-WP	AC-WP	GC-WP1	GC-WP2	GC-WP3
Push	2.133	1.771	0.521	0.612	0.512
Pull	-1.733	-1.771	-0.417	-0.266	-0.417

Table 7. Ultimate drift ratios

Load direction	Ultimate drift ratio (%)				
	Experiment	Simulation of models			
	AC-WP	AC-WP	GC-WP1	GC-WP2	GC-WP3
Push	6.476	6.476	6.476	6.476	6.476
Pull	-6.476	-6.476	-6.476	-6.476	-6.476

The envelope curves of the AC-WP, GC-WP1, GC-WP2, and GC-WP3 models are presented in Figs. 11, 12, 13, and 14, respectively. Each envelope curve shows the ultimate and yield displacement point positions determined based on a provision [29] that involved equalizing the two areas of the upper and lower curves. Using Equation (1), the processed envelope curve data resulted in the ductility ratio (μ), as given in Table 8. Due to push and pull loads, the ultimate deflection (Δ_u) was 97.14 mm for all models. All models exhibited high ductility with ratios exceeding four under push and pull loads. These ratios indicate that both the AC and GC models provided ductile behavior that fulfils the criteria for seismic design [29].

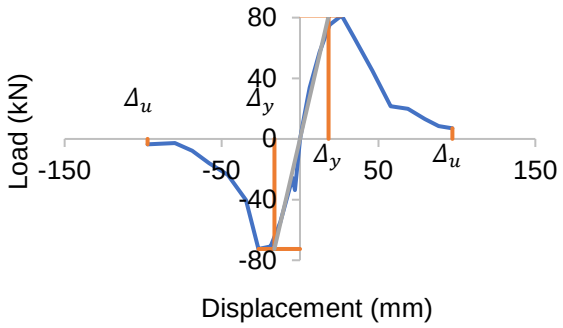

Fig. 11. Envelope curve of AC-WP model

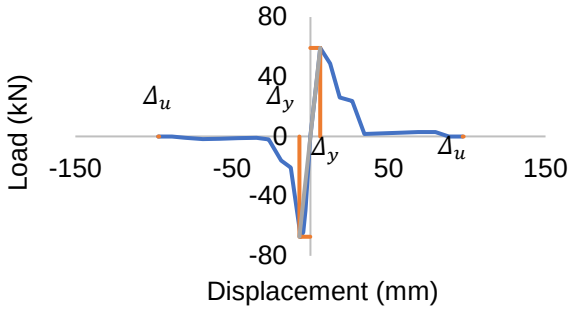

Fig. 12. Envelope curve of GC-WP1 model

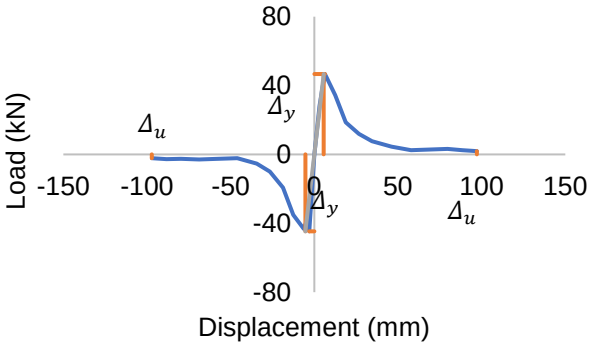

Fig. 13. Envelope curve of GC-WP1 model

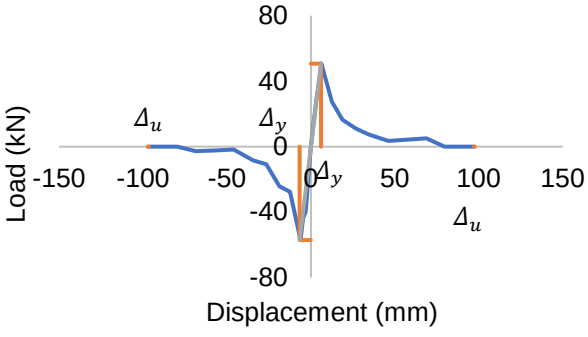

Fig. 14. Envelope curve of GC-WP3 model

Table 8. Ductility of AC-WP and GC-WP models

Model	Load direction	Ultimate deflection	Yield deflection	Ductility	Average ductility
		Δ_u	Δ_y	$\mu = \Delta_u/\Delta_y$	$\bar{\mu}$
AC-WP	Push	97.14	18.30	5.31	5.63
	Pull	97.14	16.31	5.96	
GC-WP1	Push	97.14	6.23	15.60	14.68
	Pull	97.14	7.06	13.76	
GC-WP2	Push	97.14	5.62	17.27	17.67
	Pull	97.14	5.38	18.06	
GC-WP3	Push	97.14	5.95	16.34	15.43
	Pull	97.14	6.69	14.52	

Figures 15 and 16 show the stress distribution on the AC-WP model at an ultimate drift ratio of 6.476% due to push and pull loads, respectively. Tension stresses ranging from 0.86 MPa to 4 MPa (shown in red) occurred near the model's fixed base. The foundation of the WP behaved as the fixed end of a cantilever that generated concentrated tension stresses on the WP near the fixed base. Most WP elements experienced compression stress of 2.29 MPa to tension stress of 0.86 MPa (shown in yellow). Deformation of elements due to tension stress occurred along the height of the WP on the left side (subjected to the push load), and also on the right side (subjected to the pull load).

The stress contours of GC-WP1, GC-WP2, and GC-WP3 under ultimate loads at 6.476% drift ratios are depicted in Figs. 17-22. All GC-WP models exhibited a narrower range of compression to tension stresses than their AC-WP counterpart, owing to the absence of fiber textile strengthening present in the AC [13] that supported more flexural behavior [30,31]. Figure 17 shows the stress contour of GC-WP1 (two horizontal openings) owing to the push load. This condition resulted in higher compression stresses due to the pressure exerted by the push load on the lower-right section of the wall. The compressive stresses ranged from -1.86 MPa to -0.14 MPa. Most elements experienced stresses ranging from -0.14 MPa (compression) to 0.43 MPa (tension). Figure 18 depicts GP-WP1 under the condition of ultimate pull load where compression stresses occurred mainly near the fixed base.

Figures 19 and 20 show the stress contours of GC-WP2, which were concentrated on the right side of the WP openings owing to the push and pull loads, respectively. The stress contour in the middle of the WP was a critical path for the lateral force, which propagated to the bearing area. Although GC-WP2 and GC-WP3 exhibited the same range of compressive stresses, differences dependent on the positions of the openings were observed in the area with the highest compressive stress range (-1.29 MPa to -0.71 MPa).

The vertically positioned openings affected the broader area of the stress contour owing to the lower stiffness of GC-WP3 compared with that of GC-WP1 under cyclic loads. This behavior is depicted in Figs. 21 and 22. Figure 21 shows that GC-WP3 experienced higher stresses than GC-WP2 near the fixed base. Figure 22 shows that the compressive stresses ranging from -1.86 to -0.14 MPa propagated primarily between the two vertical openings in the middle of the wall. The lateral loads were distributed along the height of the WP. The critical areas of GC-WP3 were wider than those of GC-WP2. Higher stresses occurred on the lower-left section of the wall.

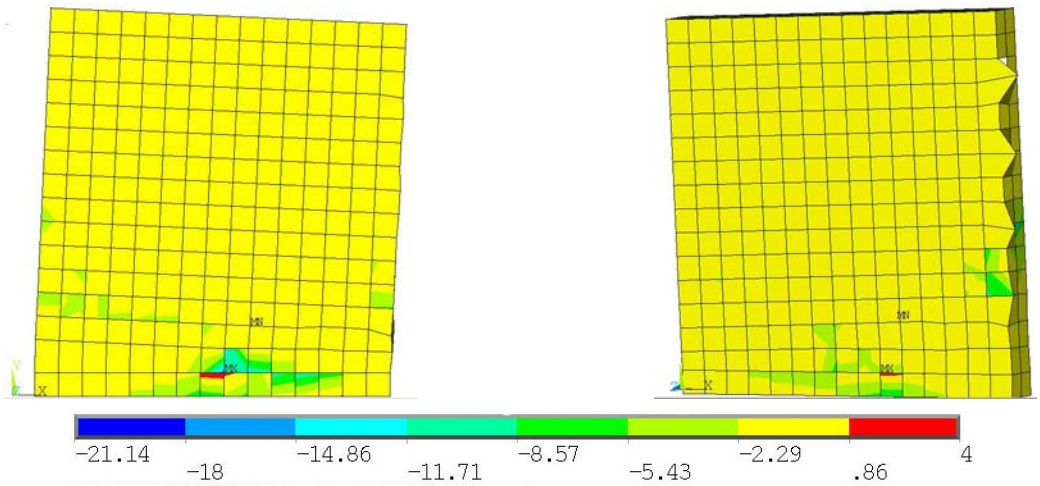

Fig. 15. Stress contour of AC-WP under ultimate push load

Fig. 16. Stress contour of AC-WP under ultimate pull load

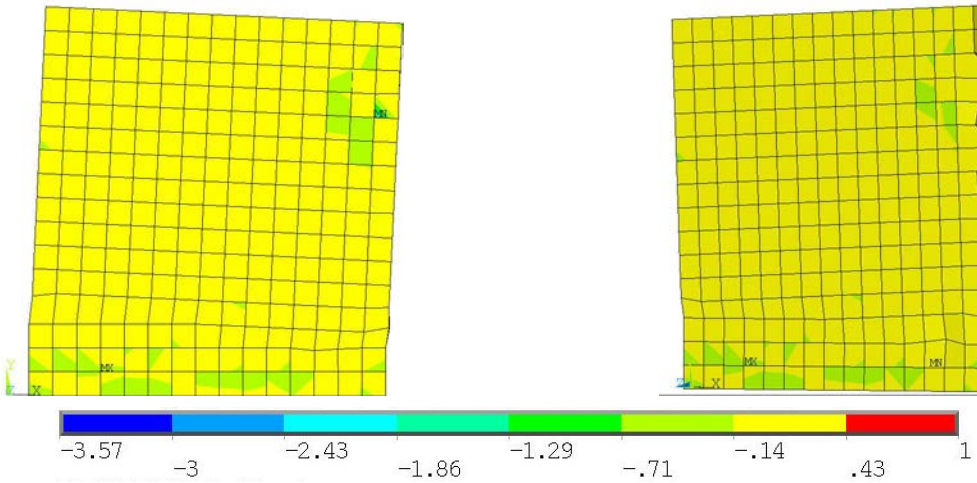

Fig. 17. Stress contour of GC-WP1 model under ultimate push load

Fig. 18. Stress contour of GC-WP1 under ultimate pull load

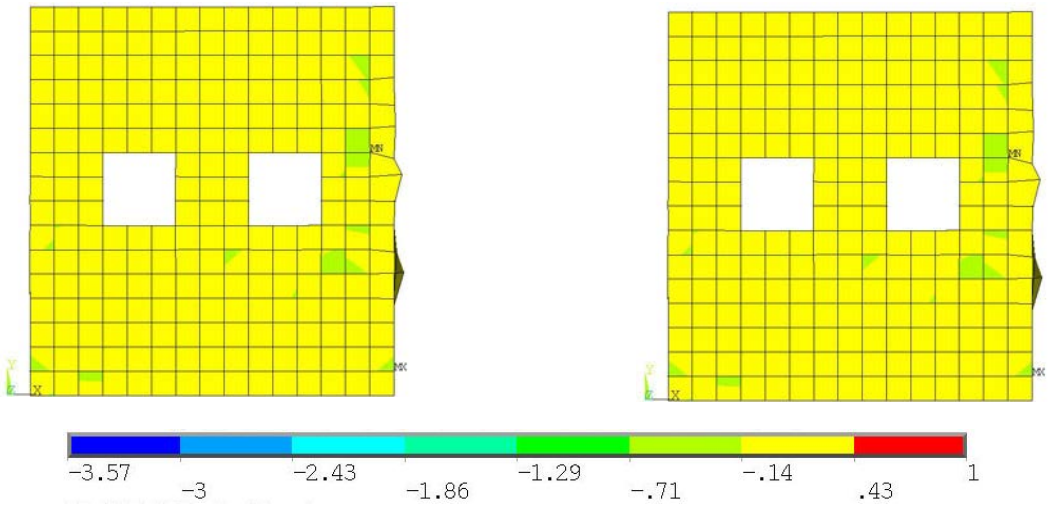

Fig. 19. Stress contour of GC-WP2 model under ultimate push load

Fig. 20. Stress contour of GC-WP2 under ultimate pull load

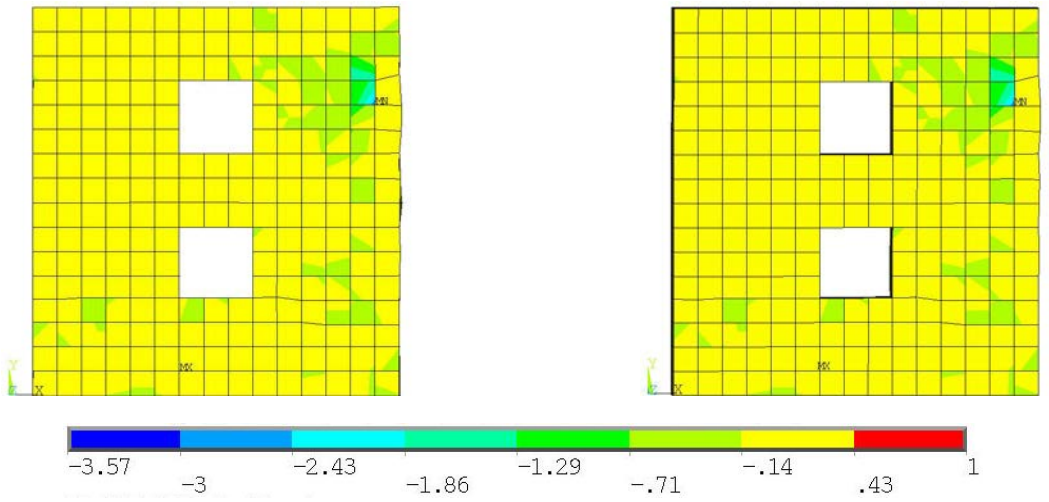

Fig. 21. Stress contour of GC-WP3 model under ultimate push load

Fig. 22. Stress contour of GC-WP3 under ultimate pull load

In this study, the numerical modeling of the AC-WP served as a verification process. The GC-WP1, GC-WP2, and GC-WP3 models with various openings provided information on the performance of WP structures using GC. The analysis revealed that the GC-WP models achieved high ductility in resisting lateral cyclic loads. The ultimate lateral loads achieved by the AC-WP caused greater compressive and tensile stresses than those seen in any of the GC-WP models. The location of the openings on the GC-WP models influenced the distribution and magnitude of the compressive stresses. The analysis results provided information about the potential of GC materials for structural

WPs capable of bearing cyclic lateral loads. Simulations by numerical modeling did not provide any information about crack propagation. Further study is needed to support these findings, particularly experimental work (parametric research) to provide empirical data regarding the performance of GC structural WPs.

4 CONCLUSION

Numerical modeling was performed using ANSYS software to investigate the performances of an AC-WP model and GC-WP models. The conclusions obtained are as follows:

1. The differences between the experimental and numerical modeling values due to push and pull loads were 6.758% and 9.871%, respectively. These values are below 10%, which signifies high accuracy. However, further parametric studies should be performed.
2. The solid GC-WP1 model achieved the highest maximum lateral load compared with the GC-WP2 (two horizontal openings) and GC-WP3 (two vertical openings) models, owing to GC-WP1 having the highest stiffness. The lower lateral loads achieved by GC-WP2 compared with GC-WP3 were due to the reduced stiffness caused by the two horizontal openings. The stiffness behavior resulted in maximum lateral push loads of 90 kN, 81.401 kN, 73.994 kN, 58.686 kN, 64.418 kN, and pull loads of -67 kN, -72.559 kN, -67.225 kN, -50.904 kN, -57.069 kN for the WP specimen, AC-WP, GC-WP1, GC-WP2, and GC-WP3 models, respectively.
3. The average high ductility ratios of the AC-WP, GC-WP1, GC-WP2, and GC-WP3 models were 5.632, 14.681, 17.665, and 15.432, respectively. This indicates that the ductility behavior exhibited by the GC satisfies the seismic design requirements.
4. Unlike the GC-WP models, the AC-WP model experienced tensile stress owing to the resisted highest lateral loads. The compressive stresses exhibited by the AC-WP and all GC-WP models were lower than the compressive strengths of the AC and GC materials.
5. This investigation's results provide valuable information on the behavior of geopolymer WPs that is useful for future research. However, areas for improvement remain, including the need for more information on crack propagation in WPs. Further parametric research can provide empirical information about the performance of GC WPs.

5 RECOMMENDATIONS

Parametric studies are needed to investigate the potential of geopolymer concrete as a material for structural WPs, obtain empirical data, and comprehend the structure's performance in terms of its ability to withstand lateral cyclic loads, and its energy dissipation, ductility, and crack propagation patterns.

6 ACKNOWLEDGMENTS

The authors really appreciate the generous support provided for this research by Sriwijaya University.

7 REFERENCES

[1] Asadi, I., Baghban, M.H., Hashemi, M., Izadyar, N., Sajadi, B. (2022). Phase change materials incorporated into geopolymer concrete for enhancing energy efficiency and sustainability of buildings: A review. Case Studies in Construction Materials, vol. 17, e01162, pp, 1-17, DOI: 10.1016/j.cscm.2022.e01162.

[2] Masoule, M.S.T., Bahrami, N., Karimzadeh, M., Mohasanati, B., Shoaei, P., Ameri, F., Ozbakkaloglu, T. (2022). Lightweight geopolymer concrete: A critical review on the feasibility, mixture design, durability properties, and microstructure. Ceramics International, vol. 48, pp. 10347–10371, DOI: 10.1016/j.ceramint.2022.01.298.

[3] Nergis, D.D.B., Abdullah, M.M.A.B., Vizureanu, P., Tahir, M.F.M. (2018). Geopolymers and Their Uses: Review. IOP Conference Series: Materials Science and Engineering, vol. 374, 012019, DOI: 10.1088/1757-899X/374/1/012019.

[4] Ouni, M.H.E., Raza, A., Haider, H., Arshad, M., Azab, M., Elhag, A.B. (2023). Behavior of alkali-activated coal ash basalt fiber-reinforced geopolymer nanocomposite incorporated with nano sodium oxide. Materials Letters, vol. 335, 133850, DOI: 10.1016/j.matlet.2023.133850.

[5] Raza, A., Azab, M., Baki, Z.A., Hachem, C.E., Ouni, M.H.E., Kahla, N.B. (2023). Experimental study on mechanical, toughness, and microstructural characteristics of micro-carbon fiber-reinforced geopolymer having nano TiO_2. Alexandria Engineering Journal, vol. 64, pp. 451–463, DOI: 10.1016/j.aej.2022.09.001.

[6] Mao, Y., Hwang, H-J., Du, Y., Su, J., Hu, X., Liu, Y., Shi, C. (2022). Bond and anchorage performance of beam flexural bars in beam-column joints using slag-based geopolymer concrete and their effect on seismic performance. Engineering Structures, vol. 273, 115062, DOI: 10.1016/j.engstruct.2022.115062.

[7] Yang, Y., Fang, S., Feng, W., Wan, S., Li, L., Tang, Y. (2023). Flexural and compressive performance of BFRP-reinforced geopolymer sea-sand concrete beams and columns: Experimental and analytical investigation. Composite Structures, vol. 318, 117089, DOI: 10.1016/j.compstruct.2023.117089.

[8] Choudhury, A.H., Laskar, A.I., (2021). Rehabilitation of substandard beam-column joint using geopolymer. Engineering Structures, vol. 238, 112241, DOI: 10.1016/j.engstruct.2021.112241.

[9] Huang, J-Q., Kumar, S., Dai, J-G. (2023). Flexural performance of steel-reinforced geopolymer concrete one-way slabs: Experimental and numerical investigations. Construction and Building Materials, vol. 366, 130098, DOI: 10.1016/j.conbuildmat.2022.130098.

[10] Zhang, H.Y., Liu, H.Y., Kodur, V. Li, M.Y., Zhou, Y. (2022) Flexural behavior of concrete slabs strengthened with textile reinforced geopolymer mortar. Composite Structures, vol. 284, 115220, DOI: 10.1016/j.compstruct.2022.115220.

[11] Cholostiakow, S., Koutas, L.N., Papakonstantinou, C.G. (2023). Geopolymer versus cement-based textile-reinforced mortar: Diagonal compression tests on masonry walls representative of infills in RC frames. Construction and Building Materials, vol. 373, 130836, DOI: 10.1016/j.conbuildmat.2023.130836.

[12] Buyuktapu, M., Maras, M.M. (2023). Optimization of production parameters of novel hybrid fiber-reinforced geopolymer mortar: Application in masonry walls. Structures, vol. 53, pp. 1300–1317, DOI: 10.1016/j.istruc.2023.05.031.

[13] Arslan, M.E., Celebi, E. (2019). An Experimental Study on Cyclic Behavior of Aerated Concrete Block Masonry Walls Retrofitted with Different Methods. Construction and Building Materials, vol. 200, pp 226–239, DOI: 10.1016/j.conbuildmat.2018.12.132.

[14] Kumar, S., Chen, B., Xu, Y., Dai, J.G. (2022). Axial-flexural behavior of FRP grid-reinforced geopolymer concrete sandwich wall panels enabled with FRP connectors. Journal of Building Engineering, vol. 47, 103907, pp 1-21, DOI: 10.1016/j.jobe.2021.103907.

[15] Zhong, Y.C., Xiong, F., Ran, M.M., Chen, J., Ge, Q., Lu, Y. (2022). Seismic behavior of a novel bolt-connected horizontal joint for precast RC wall panel structures: Experimental and numerical analysis. Journal of Building Engineering, vol. 52, 104451, pp 1-22, DOI: 10.1016/j.jobe.2022.104451.

[16] Zhang, C., Wu, J., Huang, W., Wang, H., Gao, J. (2021). Experimental and numerical study on seismic performance of semi-rigid steel frame infilled with prefabricated damping wall panels. Engineering Structures, vol. 246, 113056, pp 1-15, DOI: 10.1016/j.engstruct.2021.113056.

[17] Abdel-Jaber, M., El-Nimri, R. (2022). Comparative investigation, numerical modeling, and buckling analysis of one-way reinforced concrete wall panels. Results in Engineering, vol. 14, 100459, pp 1-10, DOI: 10.1016/j.rineng.2022.100459.

[18] Kulkarni, A., Shafei, B. (2021). Ultra-high performance concrete building wall panels engineered to resist windborne debris impact. Journal of Building Engineering, vol. 42, 103004, pp 1-14, DOI: 10.1016/j.jobe.2021.103004.

[19] Zulfiati, R., Saloma, Idris, Y. (2019). Mechanical Properties of Fly Ash-Based Geopolymer with Natural Fiber. IOP Conf. Series: Journal of Physics: Conf. Series 1198, 082021, DOI: 10.1088/1742-6596/1198/8/082021.

[20] Fragomeni, S., Doh, J.H., Lee, D.J. (2012). Behavior of Axially Loaded Concrete Wall Panels with Openings: An Experimental Study. Advances in Structural Engineering, vol. 15, no. 8, pp. 1345-1358, DOI: 10.1260/1369-4332.15.8.1345.

[21] Applied Technology Council. (2007). FEMA 461 Interim Testing Protocols for Determining the Seismic Performance Characteristics of Structural and Non-structural Components. Federal Emergency Management Agency, Redwood City California, http://www.atcouncil.org/pdfs/FEMA461.pdf.

[22] ANSYS Inc. (2019). ANSYS 19 Mechanical APDL, Canonsburg, Pennsylvania.

[23] Budiono, B., Dewi, N.T.H., Lim, E. (2019). Finite Element Analysis of Reinforced Concrete Coupling Beams. Journal of Engineering and Technological Sciences, vol. 51, no. 6, pp. 762-771, DOI: 10.5614/j.eng.technol.sci.2019.51.6.2.

[24] Nurjannah, S.A., Saloma, Idris, Y., Usman, A.P., Juliantina, I., Aprilia, C. (2022). The Behavior of Interior Beam-Column Joint Models Using Self-Compacting Concrete with Variations of Shear Reinforcement Subjected to Cyclic Lateral Loads. Civil Engineering and Architecture, vol. 10, no. 4, pp. 1574-1589, DOI: 10.13189/cea.2022.100427.

[25] Abusafaqa, F.R., Samaaneh, M.A., Dwaikat, M.B.M. (2022). Improving ductility behavior of sway-special exterior beam-column joint using ultra-high performance fiber-reinforced concrete. Structures, vol. 36, pp 979–996, DOI: 10.1016/j.istruc.2021.12.059.

[26] Nurjannah, S.A., Saloma, Usman, A.P., Wibowo, M.L.P.P. (2022). A Numerical Study of the Comparison of Normal Concrete and Light Weight Concrete Exterior Beam-Column Joints Behavior to Cyclic Lateral Loads. Journal of Applied Engineering Science, vol. 20, no. 3, pp. 765-777, DOI: 10.5937/jaes0-36140.

[27] Wu, H., Zhuang, X., Zhang, W., Zhao, Z. (2022). Anisotropic ductile fracture: Experiments, modeling, and numerical simulations. Journal of Materials Research and Technology, vol. 20, pp 833-856, DOI: 10.1016/j.jmrt.2022.07.128.

[28] Nurjannah, S.A., Saloma, Yulindasari, Aminuddin, K.M., Chuhairy, G. (2023). The analysis of numerical self-compacting concrete wall panel models with variations of shear reinforcement. Engineering Solid Mechanics, vol. 11, pp. 89-102, DOI: 10.5267/j.esm.2022.8.002.

[29] American Society of Civil Engineers. (2000). Prestandard and Commentary for the Seismic Rehabilitation of Buildings, Federal Emergency Management Agency 356, Washington D.C.

[30] Batarlar, B., Saatci, S. (2022). Numerical investigation on the behavior of reinforced concrete slabs strengthened with carbon fiber textile reinforcement under impact loads. Structures, vol. 41, pp. 1164–1177, DOI: 10.1016/j.istruc.2022.05.057.

[31] Zhang, Q., Yang, Q-C., Li, W-J, Gu, X-L., Dai, H-H. (2023). Study on model of flexure response of carbon fiber textile reinforced concrete (CTRC) sheets with short AR-glass fibers. Case Studies in Construction Materials, vol. 18, e01791, pp. 1-20, DOI: 10.1016/j.cscm.2022.e01791.

Paper submitted: 02.04.2023.

Paper accepted: 18.08.2023.